Computational Biology and Chemistry 77 (2018) 331–342

Contents lists available at ScienceDirect

Computational Biology and Chemistry

journal homepage: www.elsevier.com/locate/cbac

Calcium interactions with Cx26 hemmichannel: Spatial association between MD simulations biding sites and variant pathogenicity

Juan M.R. Albano[a,b,1], Nahuel Mussini[a,b,1], Roxana Toriano[c,d], Julio C. Facelli[e,*], Marta B. Ferraro[a,b], Mónica Pickholz[a,b]

[a] Facultad de Ciencias Exactas y Naturales, Departamento de Física, Universidad de Buenos Aires, Argentina
[b] CONICET- Universidad de Buenos Aires, IFIBA, Buenos Aires, Argentina
[c] Facultad de Medicina, Departamento de Ciencias Fisiológicas, Laboratorio de Biomembranas, Buenos Aires, Argentina
[d] CONICET - Universidad de Buenos Aires, IFIBIO Houssay, Buenos Aires, Argentina
[e] Department of Biomedical Informatics, The University of Utah, 421 Wakara Way, Suite 140, Salt Lake City, UT 84108, USA

ARTICLE INFO

Keywords:
Connexin
Molecular dynamics
POPC
Variant annotation

ABSTRACT

Connexinophaties are a collective of diseases related to connexin channels and hemichannels. In particular many Cx26 alterations are strongly associated to human deafness. Calcium plays an important role on this structures regulation. Here, using calcium as a probe, extensive atomistic Molecular Dynamics simulations were performed on the Cx26 hemichannel embedded in a lipid bilayer. Exploring different initial conditions and calcium concentration, simulation reached ~4 μs. Several analysis were carried out in order to reveal the calcium distribution and localization, such as electron density profiles, density maps and distance time evolution, which is directly associated to the interaction energy. Specific amino acid interactions with calcium and their stability were capture within this context. Few of these sites such as, GLU42, GLU47, GLY45 and ASP50, were already suggested in the literature. Besides, we identified novel calcium biding sites: ASP2, ASP117, ASP159, GLU114, GLU119, GLU120 and VAL226. To the best of our knowledge, this is the first time that these sites are reported within this context. Furthermore, since various pathologies involving the Cx26 hemichannel are associated with pathogenic variants in the corresponding CJB2 gene, using ClinVar, we were able to spatially associate the 3D positions of the identified calcium binding sites within the framework of this work with reported pathogenic variants in the CJB2 gene. This study presents a first step on finding associations between molecular features and pathological variants of the Cx26 hemichannel.

1. Introduction

Multicellular organisms require multiple types of inter-cellular communication in order to respond in an organized way - in either tissue or organ - to stimuli of the organism itself or from the environment that surrounds it (Trosko and Ruch, 1998; Vinken, 2015; Mab et al., 2006; Evans and Martin, 2002; Peracchia, 2004). The most common and ubiquitous form of this intercellular communication in animal tissues is through the Gap Junction Channels (GJCs) (Vinken, 2015; Mab et al., 2006; Evans and Martin, 2002; Hanner et al., 2010; Scott et al., 2012). GJCs (Fig. 1) are structures that connect cells allowing the direct exchange of ions and molecules with a molecular weight cut-off of about 1 kDa (Nielsen et al., 2012). GJCs are involved in many cellular processes determining the normal physiology of an organism, such as cell proliferation, differentiation, migration, and apoptosis (Vinken, 2015; Scott et al., 2012; Nielsen et al., 2012; Figueroa and Duling, 2009; Elias et al., 2007). Multiple pathologies and developmental disorders, such as hearing loss, skin diseases, peripheral and central neuropathic disorders, lens cataracts (Cx26, Cx30) and cardiac arrhythmias (Cx40), have been associated with different dysfunctions of hemichannels and GJCs (García et al., 2016; Srinivas et al., 2017; Delmar and Makita, 2012). Many of these pathologies are associated to specific genetic variants that change the Cx amino acid sequence (García et al., 2016; Srinivas et al., 2017). For example, two clinical phenotypes were associated to hearing loss due to Cx26 hemichannel malfunction (Kelsell et al., 1997) and a heterozygous missense mutation was identified in a family with dominant deaf-mutism and palmoplantar keratoderma (Heathcote et al., 2000).

* Corresponding author.
E-mail address: julio.facelli@utah.edu (J.C. Facelli).
[1] These authors contributed equally to this work.

https://doi.org/10.1016/j.compbiolchem.2018.11.004
Received 21 May 2018; Received in revised form 8 July 2018; Accepted 8 November 2018
Available online 12 November 2018
1476-9271/

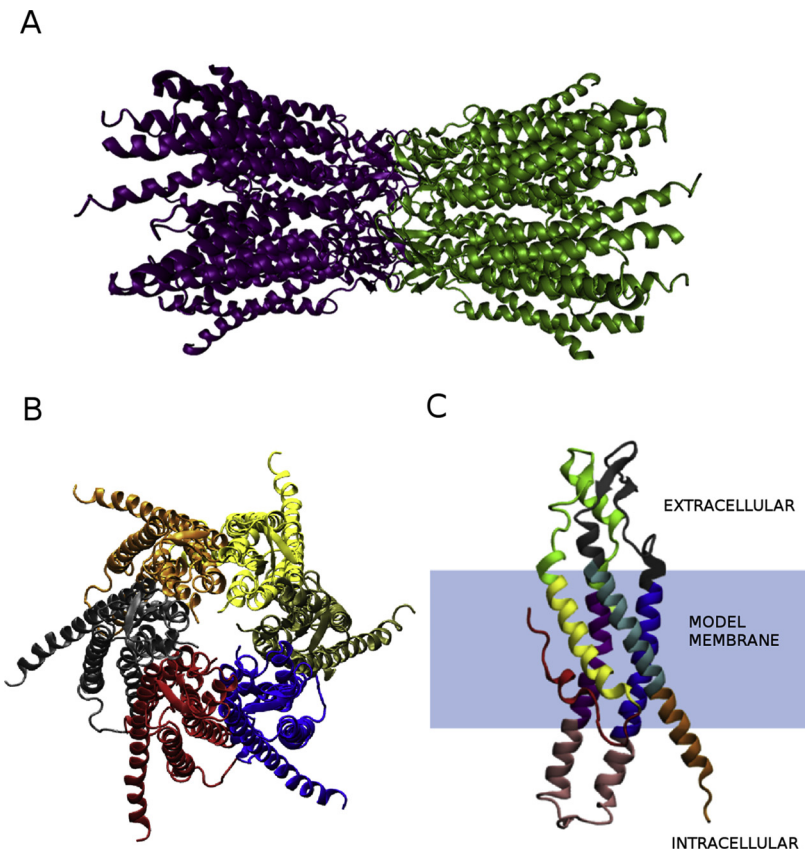

Fig. 1. Schematic Representation of the Cx26 structures. A- Gap Junction channel. Each connexon shown in different color. B- Connexon structure. Each connexin has a different color. C- Connexin structure and its domains Transmembrane Segments TM1 (Yellow), TM2 (Violet), TM3 (Blue), TM4 (Light Blue); Extracellular Loops E1 (Green), E2 (Black); Intra-cellular C-terminal CT (Orange); Intra-cellular Loop CL (Pink), and Intra Pore Segment NTH (Red) (For interpretation of the references to colour in this figure legend, the reader is referred to the web version of this article).

The GJCs are constituted by the head-to-head non-covalent coupling of two hexameric oligomers named connexons, each one of them placed in the plasma membrane of adjacent cells (Fig. 1) (Beyer and Berthoud, 2017). The connexons can also work as hemichannels providing a direct and highly regulated transmembrane communication pathway (Bennett et al., 2003; Hung and Yarovsky, 2011; Lopez et al., 2018). The monomer subunit of the hexameric arrangement is the Connexin (Cx), a highly-conserved sequence protein constituted by four hydrophobic transmembrane segments named TM1 to TM4 (Fig. 1) (Pantano et al., 2008; Yeager and Harris, 2007). The N-terminal domain of Cx is inside the cell and it is located within the channel pore determining the polarity of the gap junction channel (Nielsen et al., 2012). Thus, the conformational flexibility of this region is crucial for proper regulation of the channel (Kyle et al., 2008). The C- terminal domains and one of the connecting loops from the Cx26 are also inside the cell, whereas the two others are outside the cell. These last extracellular loops are essential for the docking between connexons. GJCs and connexons hemichannels are sensitive to several intracellular and extracellular factors affecting a variety of physiological processes and pathological states. One of these factors is Ca^{2+} concentration, which ranging from 2 mM extracellular to 10–100 nM intracellular, is a key element in the regulation of GJC conductance and therefore a driver of multiple physiological properties (Peracchia, 2004; Lopez et al., 2018; Zonta et al., 2012a; Zhang et al., 2005).

A milestone in the field of molecular modelling of connexons occurred when the crystal structure of the GJC of connexin 26 (Cx26) was reported with a resolution of 3.5 Å (Maeda et al., 2009). GJCs were crystalized with and without Ca^{2+} (Bennett et al., 2016) and both structures were virtually identical, except from the large structural changes observed in close proximity of Ca^{2+} binding sites. From the structural knowledge of these systems, several Molecular Dynamics (MD) simulations experiments of the human Cx26 in multiple environments have been carried out (Pantano et al., 2008; Zonta et al., 2012a, a; Kwon et al., 2012; Araya-Secchi et al., 2014). In particular, MD simulations have been used to study Ca^{2+} binding sites at the interface between adjacent subunits close to the extra cellular connexons junction. The importance of this is captured in a recent review article on structure-function relationships on GJCs channel by modelling and simulations by Villanelo el al. (Villanelo et al., 2017).

In this work, using calcium as a probe at high concentrations, MD simulations were used to identify potential calcium binding sites of a hemichannel embedded in a model membrane. The MD simulations were conducted taking into account four different cases. These simulations allowed us to explore the various specific amino acids strongly interacting with calcium ions and their dynamics. Furthermore, the position of these amino acids was spatially associated to known pathogenic mutations, using the ClinVar database (Landrum et al., 2014). In the next sections, we describe the four systems studied and the methodology used in the MD simulations (Albano et al., 2018); the results of the simulations and their association with ClinVar annotations. In the Discussion section, we compare our findings with those from the literature. The Conclusions summarize our major findings and discuss how the approach used here may be extended to other systems.

2. Materials and methods

MD simulations were performed using the GROMACS 5.0.4 software package (Abraham et al., 2015) with the CHARMM36 force-field (Best et al., 2012) and the TIP3P model for water (Wu et al., 2006; Mahoney and Jorgensen, 2000). After 10 ns of equilibration, MD simulations were carried out for 500 ns production runs within the NPT (constant number of particles, temperature, and pressure) ensemble. The system was coupled to a temperature bath with a reference temperature of 310 K and a relaxation constant of 0.1 ps. Temperature was kept constant using the Nosé-Hoover thermostat (Nosé (1984); Hoover (1985)) with a coupling constant of 6.0 ps and the pressure was equilibrated at 1 bar using the Parrinello-Rahman barostat (Parrinello and Rahman, 1982) with a coupling constant of 6.0 ps and compressibility of

$4.5 \times 10-5bar-1$. The electrostatic interactions were taken into account using the Particle Mesh Ewald (PME) version of the Ewald sums (Ewald, 1921; Herce et al., 2007) considering a real space cut off of 1.0 nm, a grid spacing of 0.12 nm and a cubic interpolation. In all the simulations the Van der Waals interactions were cut off at 1.0 nm (Hess et al., 2008). The time step for the integration of the equation of motion was 2 fs. The non-bonded list was updated every 10 steps. All simulations were performed without any constrains. The simulations were performed in the Center of High Computer Performance (CHPC) at the University of Utah, using 120 cores of commodity processors. The figures were obtained using Visual Molecular Dynamics (Humphrey et al., 1996) software (VMD from University of Illinois at Urbana-Champaign, IL, USA), Chimera (Pettersen et al., 2004) and Grace (http://plasma-gate.weizmann.ac.il/Grace/) software packages.

The simulated systems were based on a Cx26 connexon embedded into a POPC bilayer. The protein structure of the Cx26 was the 3.5 Å X-ray structure of the Connexon Cx26 obtained by Maeda et al. (Maeda et al. (2009)) and completed with homology modelling techniques (Hung and Yarovsky, 2011). The protein structure was embedded into a 500 1-palmitoyl-2-oleoylsn-glycero-3-phosphocholine (POPC) (250 in each leaflet) lipid bilayer by the replacement method and using the web based software CHARMM-GUI (Jo et al., 2008; Wu et al., 2014). POPC lipids are broadly used in biomimetic studies and it is one of the most used systems in this kind of membrane protein MD simulations (Zonta et al., 2012b). The assembled systems were solvated with sufficient number of water molecules (> 46,000) to ensure proper hydration of the lipid bilayer and to prevent the interaction of the protein with itself (~25 Å) with periodic boundary conditions (PBC). A sodium chloride solution was used to neutralize the net and local charges of the system.

Even for these big systems, physiological calcium concentration corresponds to 0.1–1.7 calcium atoms, which may be insufficient to identify biding sites within a reasonable simulation time. To overcome this, we considered calcium concentrations higher than physiological ones to obtain as broad sample as possible of binding sites. We performed three simulations varying the concentration of calcium and buffer ions, initially placed into the water phase. The calcium ions were randomly placed in the simulation box using a water replace method available in the GROMACS simulation package. These three studies will be referred to as CA−r (with r = 0, 0.04 and 0.1, corresponding to Ca^{2+} concentration none, 0.04 M and 0.1 M, respectively). We carried out an additional simulation at a calcium concentration of 0.1 M, were initially eight Ca^{2+} ions were placed inside the connexon pore, *i-CA-0.1*. In this case, we replaced random waters and ions present at different sections of the pore editing the initial configurations. All the simulations were run in duplicates.

In Table 1 we summarized the characteristics of each of the systems described above, including the number of atoms, number of different ions and characteristic simulation run times.

Known pathogenic variants of Cx26 (CJB2 gene) were extracted from ClinVar (https://www.ncbi.nlm.nih.gov/clinvar/) (Landrum et al., 2014), which is the most comprehensive and authoritative source of annotated human variants with known clinical impact. The search for variants was performed using the web interphase of ClinVar in April 17th of 2017 and the variants were recorded manually and assigned against the same Cx26 sequence as used in the simulations (see Discussion section for details). Mutation sites that are far removed from calcium binding sites in the protein sequence may be in their physical proximity and therefore able to change calcium binding ability at the site. To study this issue, we labelled in the Cx26 structure the calcium binding sites and the mutations sites using a pairwise approach and visually identified potential regions of interest.

Table 1
Summary of the four simulated systems considered in this study.

System name	N of atoms	Nº of Ca2+	Nº of Na+	Nº of Cl-	Run time [&]
CA-0	229,030	0	150	204	500 ns
CA-0.04	229,138	36	150	276	500 ns
CA-0.1	229,285	85	150	374	500 ns
i-CA-0.1	229,285	85	150	374	500 ns

[&] Average run times are 25 ns per day using 120 cores for systems with 230,000 sites.

3. Results and discussions

In order to assess the protein structural stability and dynamics during the simulations, we calculated the Root Mean Square Deviation (RMSD) of the protein alpha carbons (Cα) (Kabsch, 1976) and Root Mean Square Fluctuation (RMSF) of each residue (Vendome et al., 2011), using as a reference the initial configuration structure of the connexon (Hung and Yarovsky (2011)). Fig. 2 compares the RMSD of the CA − 0 (green), CA − 0.04 (red) and CA − 0.1 (black) systems, over 500 ns simulations. The RMSD results for the replicas are presented in Fig. S1 of the Supplementary Material. All RMSDs are compatible with a highly stable protein backbone during the simulation time after equilibration (Capener and Sansom, 2002). The order of magnitude of the drift from the initial structure was approximately 5 Å for all systems, but it is apparent from Fig. 2 that the systems are not fully equilibrated at the beginning of the 500 ns production runs. Therefore, all the analysis presented here disregarded the first 50 ns of the production run, i.e. all average quantities where calculated using the last 450 ns of the simulations to eliminate any transient effects on the results presented here.

To gather insight on the relative fluctuation of different regions within each Cx26 structure we evaluated the RMSF of the backbone of each amino acid residue in the four different chains of the structure (Fig. 3) for the last 450 ns of the production runs. RMSF results on the replicas are presented in Fig. S2 of the Supplementary Material.

Fig. 3 and S2, of the supplementary material, show the average RMSF of each residue of the six connexins chains for the three *CA-r* simulated systems. Similar fluctuations patterns are observed for the same connexins domains. The highest peak is consistently observed for the CL domain between the residues 96 and 132. The fluctuations observed within the regions of residues 210–226 and 1–19 correspond to the CT and NTH terminal domains. As expected, the CT and CL domains located outside the membrane, are the most flexible ones because their lack of structural constrains. The TM regions are the most stables domains since they are embedded in the lipid bilayer and organized in alpha helices, which restrict their movements (Oshima, 2014). For the NTH domain, we notice subtle differences between the *CA − 0* simulation and the others, suggesting that the Ca^{2+} ions influence the dynamical properties of this region.

The overall organization of the whole system was investigated through the calculation of the average electron density profile (EDP) along the direction normal to the bilayer (Z-axis) for the three simulations (Fig. 4) and its replicas (Fig. S3) of the supplementary material. As an example, in Fig. 4A and S3A of the supplementary material, we show the EDP of POPC (red), protein (black) and water (green) for the CA − 0.1 simulation, where Z = 0 corresponds to the bilayer center of mass. The hemichannel asymmetrical structure is reflected in the EDP distribution along the Z-axis. This asymmetry leads to a distortion of the lipid bilayer when compared with plain bilayers (Pickholz et al., 2008; Pasenkiewicz-Gierula et al., 1999) and to a high-water density at the region corresponding to the extra-cellular side of the connexon. Furthermore, contrarily to what is observed in simple lipid membranes, the density of water is different from zero in the hydrophobic region, which could be attributed to the presence of water inside the connexon pore. This was confirmed by visual inspection of the structures generated by the simulation as exemplified in Fig. S4 of the Supplementary Material.

Ion electron density profiles and z- averaged density maps (Figs. S5 to S6 and S7 to S9) of the supplementary material show that most sodium and chloride ions are widely distributed into the water phase.

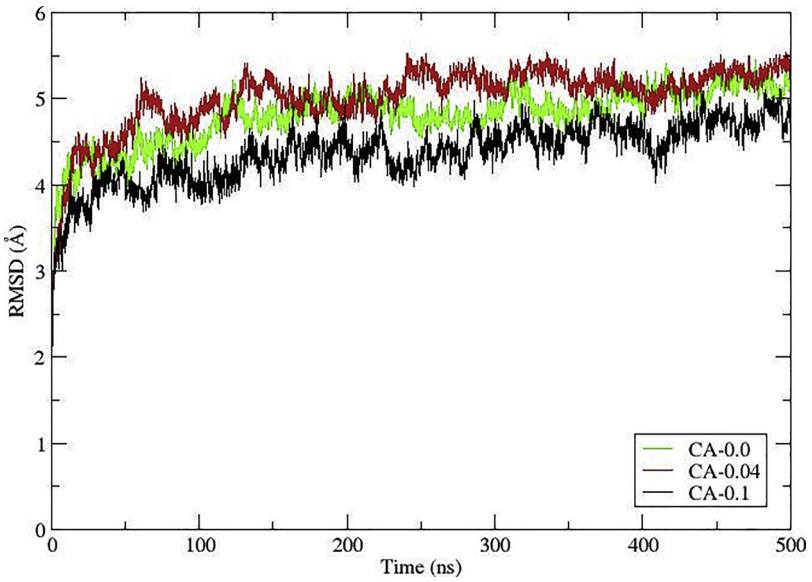

Fig. 2. RMSD calculations for the three of the systems considered in this study. Cases: A) *CA − 0* (green), B) *CA − 0.04* (red) and *CA − 0.1* (black). (For interpretation of the references to colour in this figure legend, the reader is referred to the web version of this article).

However, few of the ions are found in the outer region of the pore and some chloride ions were able to enter inside the pore during the simulation times considered here.

Fig. 4B and S3B of the supplementary material, show the calcium distribution for *CA − 0.1* (green) and *CA − 0.04* (blue) simulations and its replicas, respectively. Similar patterns are observed in both cases, with well-defined peaks (~-20Å, ~20Å and ~40 Å) at the protein edges. The first peak had the same high for both concentrations suggesting a saturation of Ca^{2+} binding sites, while the second and third peaks show an increase in their intensities with the calcium concentration. This could be explained by a difference in the total number of Ca^{2+} binding sites on each side of the protein, as is discussed below. No Ca^{2+} ions were found around at Z = 0, but in one case in the replicated system (Fig. S3B-green), it seems that a calcium ion was able to enter the pore. This is supported by the analysis of calcium density maps (S8D, S8H and S9D-S9H) and will be discussed below.

An exploratory analysis of the CX26 pore topology was carried out using the MOLE online service (Pravda et al., 2018). Through this tool, we were able to probe the pore length, characterize its bottleneck and measure different diameters. In Figs. S10 and S11 of the Supplementary Material, three snapshots of structures analysed at 100 ns (A), 300 ns (B) and 500 ns (C), for CA-0.0 and CA-01, are presented at the top of the figure along with a plot of the corresponding channel length and radius at the bottom. Our results are in good agreement with the ones reported by Batool et al. (2017) both in pore size and length. However, as it can be observed in the Fig. S11, in our work we found that high Ca^{2+} concentrations appear to be altering the intracellular topology of the pore. This issue will be explore in future work.

The Ca^{2+} interactions with specific amino acids were studied by calculating the time evolution distances between the ions and the selected atoms in the trajectories from simulations. Stable distances can be associated to stable energies, considering pair interactions between non-bonded atoms. Further information could be obtained by free energy calculation, but we consider that those calculations are outside the scope of this work, which focus in identifying potential binding sites and associate them with known pathogenic variances.

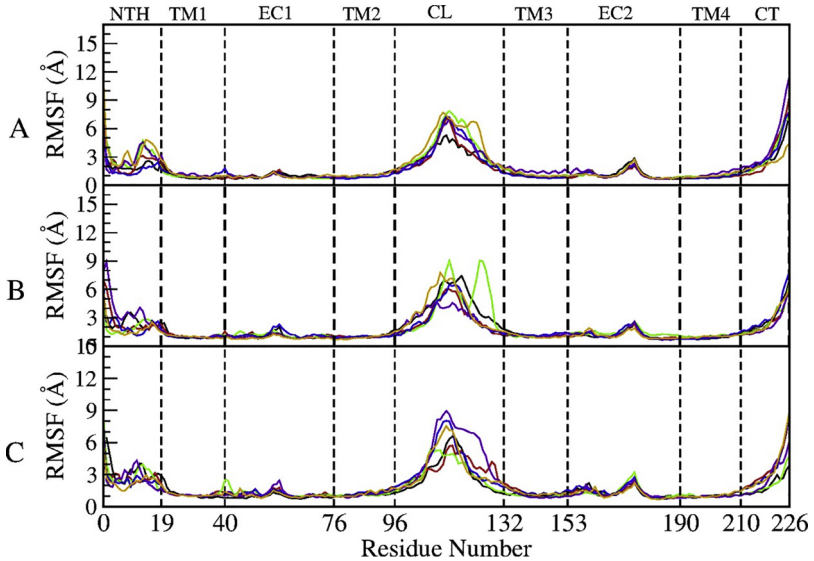

Fig. 3. RMSF of each connexin residue calculated over the simulation run. The six connexins corresponding to each case are depicted in different colors and over imposed. A) *CA-0.1* case, B) *CA-0.04* case and C) *CA-0* case. On the top, each Cx26 domain is indicated.

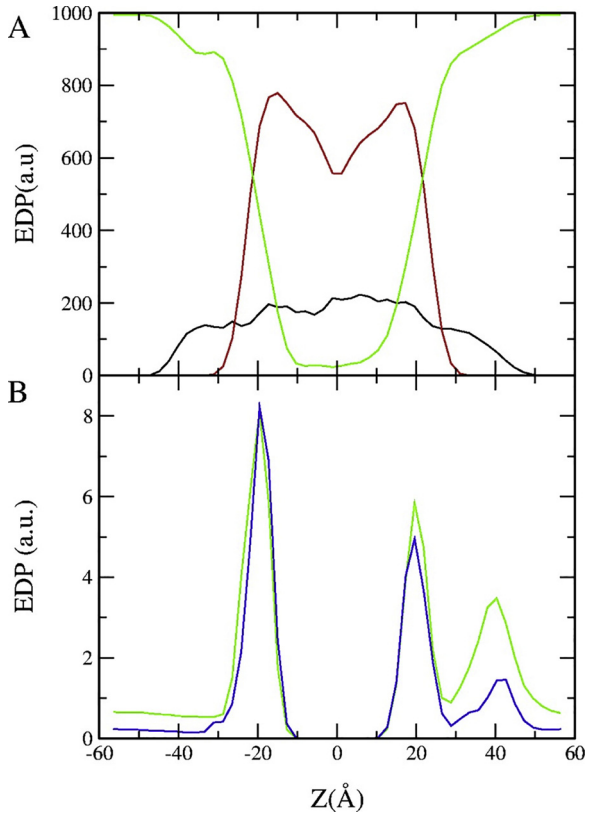

Fig. 4. Electron Density profiles. A) System *CA − 0.1*. The POPC distribution is in red, the protein distribution in black, and the water distribution in green B) Calcium EDP for the *CA − 0.04* (blue) and *CA − 0.1* (green) cases. Z = 0 corresponds to the center of the membrane, the region that corresponds to the extracellular domains of the connexon, is located between -20 and -60 Å and the intra-cellular one is between 20 and 60 Å (For interpretation of the references to colour in this figure legend, the reader is referred to the web version of this article).

Fig. 5 shows the temporal evolution of the distance between a Ca^{2+} and the two carboxylic oxygen atoms in the lateral chain of ASP50 for one of the Cx26 protomers. The distance corresponds to each oxygen atom to the calcium ion (R1 = Oxygen 1 to Ca^{2+} -red- and R2 = Oxygen 2 to Ca^{2+} -black) during the first 100 ns were the interplay between the three atoms is better observed. The distances at the initial times (t < 25 ns), are ~50 Å and exhibit large fluctuations, but after 25 ns the distances remain close to 2.35 Å, indicating a specific interaction, such as the one depicted in the inset of Fig. 5. In Fig. S12 of the Supplementary Material we present the time evolution of these distances up to 500 ns confirming the stability.

We found several other amino acids interacting with Ca^{2+} and following similar behaviors: a large initial uncorrelated fluctuation of the distances between Ca^{2+} and the lateral-chain-carboxylic oxygens followed by stabilization at a distance of ~2.35Å. These amino acids are ASP159 in the E2 domain, GLU114, ASP117, GLU119, and GLU120 in the CL domain, VAL226 in the CT domain and ASP50 in the E1 domain.

ASP50 was already identified as a calcium binding site by Zonta et al. (2012a). This finding was also supported by Lopez et al. (2013), that using mutant structures of Cx26(D50N/Y) were the ASP50 was replaced by neutral amino acids Tyrosine or Asparagine concluded that ASP50 plays a key role in the Ca_2^+ driven gating mechanism. Recently, using MD, the same authors reported that there is an electrostatic network close to the E1 region that exhibits significant disruption/rearrangement upon calcium binding (Beyer and Berthoud, 2017). In spite of the symmetry of the protein, in our simulations, the ASP50 interaction is observed only in one protomer of the connexon at a time, which may be associated with the electrostatic repulsion of a neighboring chain (Bennett et al., 2016).

We were also able to associate GLU114, GLU119 and GLU120 acids with calcium binding sites and to the best of our knowledge this is the first time that this has been reported. These three amino acids were identified to be capable of being γcarboxylated in some cells as part of post-translational modifications (Locke et al., 2006) and a mutation in GLU114 was associated with severe deafness in association with a V27I mutation (Nemoto-Hasebe et al., 2008). To the best of our knowledge, ASP 117 was not previously reported in association with a calcium binding site. This amino acid belongs to the CL region close to GLU114, GLU119 and GLU120 amino acid.

This is also the first time that a direct link between ASP159 and calcium binding is observed. Gonzalez et al. (González et al., 2006) demonstrated that human and sheep Cx26, but not the rat orthologue, are able to form open, voltage-activated hemichannels. They also showed that rat hemichannels became voltage-gated when the Aspartate found in the human and sheep replaced the Asparagine at position 159 of the rat sequence. The C-terminal residue VAL226 is also a new calcium binding site found in this study but given it´s terminal nature is possible that may not be relevant.

We identified a different total number of Ca^{2+} binding sites on each

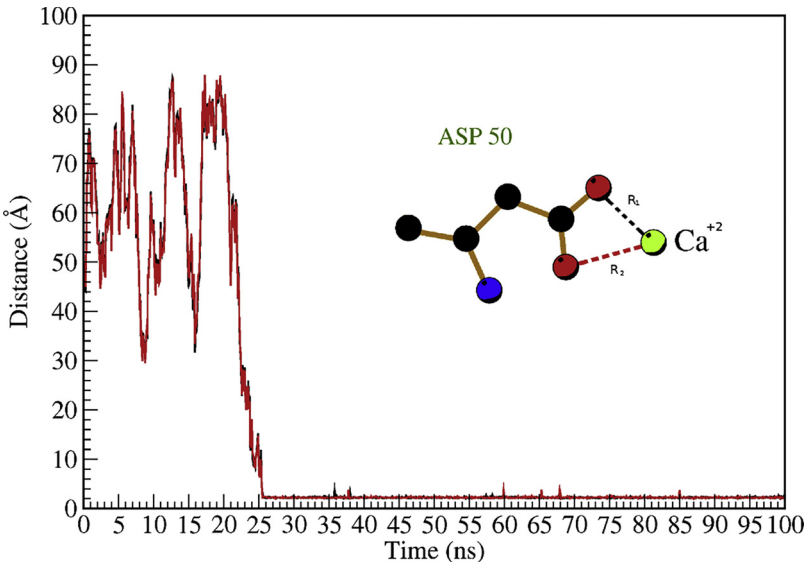

Fig. 5. Time evolution of the R1 and R2 distances: R1 and R2 are the distances between Ca^{2+} and the two carboxylic O atoms in lateral chain of ASP50. The binding distance is around 2.35Å. Inset: Schematic graph of the binding interaction between Ca^{2+} and ASP50. Both curves are superimposed.

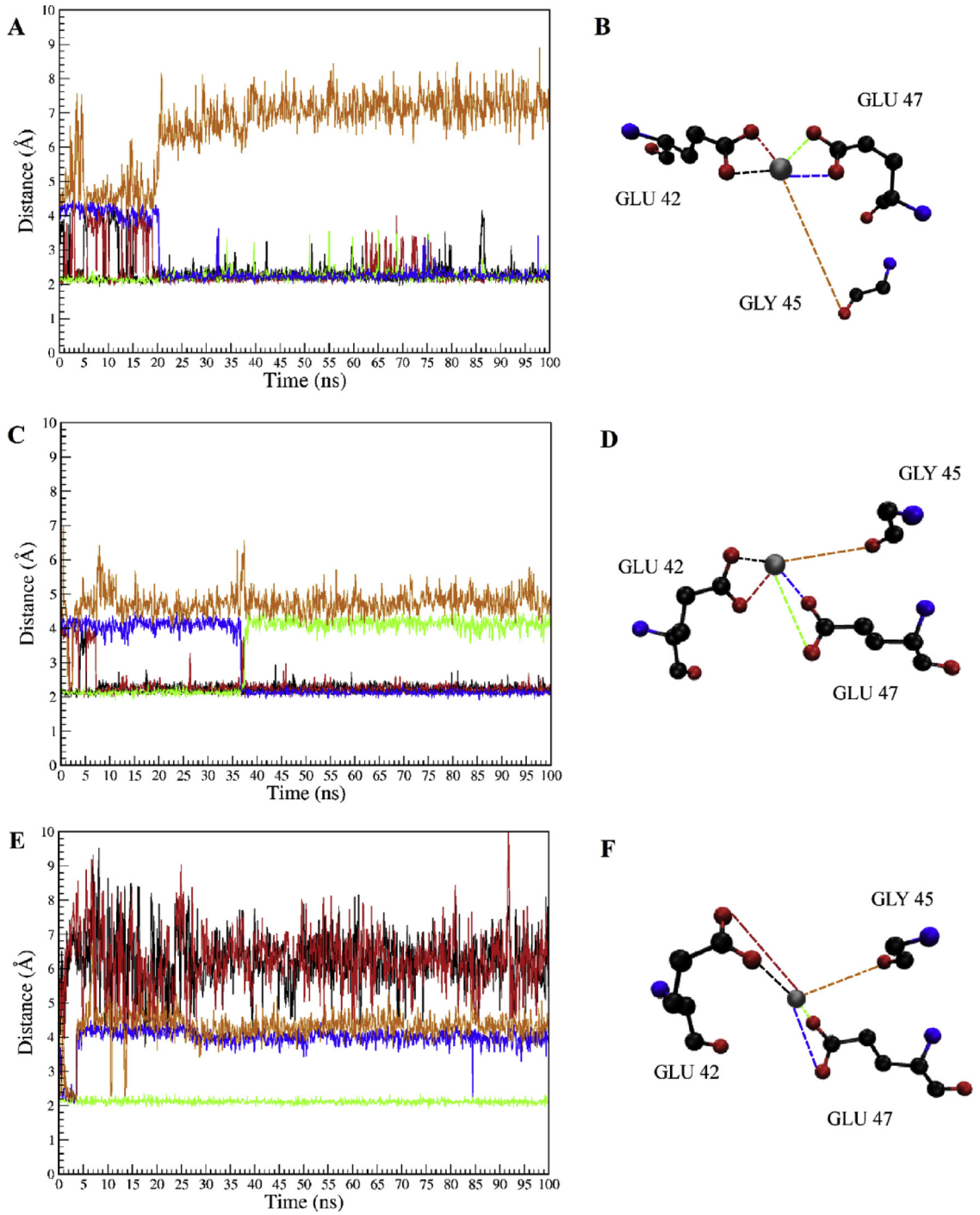

Fig. 6. Time evolution of the distances between Ca^{2+} and oxygen atoms in different amino acids. A), C) and E) distances with two carboxylic O atoms in the lateral chain of GLU42 (red and black), GLU47 (green and blue) and GLY45 (orange). B), D) and F) show a schematic representation of the corresponding arrangements, associated with the side figure (For interpretation of the references to colour in this figure legend, the reader is referred to the web version of this article).

side of the connexon: seven in the extra-cellular and thirty in the intracellular side. From Fig. 4B and S3B of the supplementary material, we observed that increasing calcium concentration leads to populating these Ca^{2+} sites corresponding to EDP peaks at ~20 Å and ~40 Å. These regions are the most flexible ones and involve ASP, GLU and VAL residues that are further away from the center of the connexon.

Under ergodic conditions all accessible binding sites will be revealed, however this is not the case for finite simulation. In order to extensively sample all possible binding sites different strategies are needed. The first one used here was to study different calcium concentration. Another strategy would be to bias the initial placement of the calcium in the simulations. In order to do so, we performed a simulation on a system –named as $i-CA-0.1$ (see Methods) - in which eight Ca^{2+} ions were placed inside the Cx26 channel and the other Ca^{2+} randomly distributed. RMSD, RMSF and membrane-protein overall organization were analyzed for the duplicate cases. The results of these calculations are presented in Figs. S13 to S15 of the supplementary material. At a first glance, no significant differences with the results discussed above for the other systems considered here were found. However, for this simulation the calcium EDP showed a new peak on the distribution at the center of the pore (Z = 0), as shown in Fig. S15B of the supplementary material. This is in correlation with the

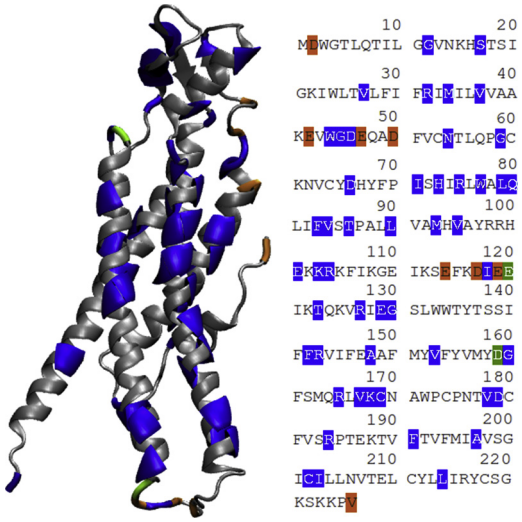

Fig. 7. Sequence of Cx26 annotated with the position for which pathogenic variants reported in ClinVar and calcium binding sites have been encountered in this study. Residues highlighted in blue, orange and green correspond to those for which pathogenic variants have been reported in ClinVar, calcium biding sites found in this study and those that meet both criteria, respectively (For interpretation of the references to colour in this figure legend, the reader is referred to the web version of this article).

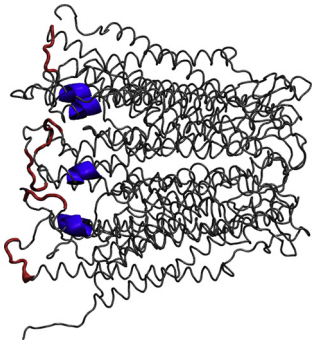

Fig. 8. Relative spatial positions of the sequences EKKR(104) in blue and EFKDIEE (120) in red. In the first sequence pathogenic mutations have been reported at GLU101, LYS103 and ARG104, whereas in the second one the positions GLU114, ASP117, GLU119 and GLU120 have been identified as calcium binding sites (For interpretation of the references to colour in this figure legend, the reader is referred to the web version of this article).

density maps analysis, where calcium density is concentrated inside the pore (Fig. S17D and S17H), a main difference with it was observed for the previous density maps. With further analysis of the simulations, we were able to identify in this area a calcium binding site involving ASP2 from two connexins. According to the literature reports (Oshima, 2014; Maeda and Tsukihara, 2011), this interaction may be physiologically relevant due to the role of ASP2 in the "plug gating mechanism", as discussed elsewhere this suggest that Ca^{2+} binding at ASP2 also may be associated with this mechanism. Visual analysis of the MD trajectories also supports this observation as exemplified in S18 of the supplementary material.

In addition to those sites described above and in agreement with an X-ray structure reported in the literature (Bennett et al., 2016), in the $i-CA-0.1$ simulation we found calcium binding sites involving GLU42, GLU47 and GLY45, which are located at the extra-cellular edge of the pore region. We were able to find three stable supra-molecular arrangements of Ca^{2+} interaction within these sites, which are shown in Fig. 6. The first arrangement (6 A, 6B) involves the oxygen atoms of the GLU42 lateral chain (red-black) and the GLU47 lateral chain (green-blue) stabilizing, at similar distances (~2.5 Å), and the oxygen of the GLY45 (orange), stabilizing at a distance between 5 Å and 7 Å. In the second arrangement (6C, 6D) the two oxygen atoms of GLU42 (red-black) are located at a stable distance (~2.3Å) of a Ca2+ and only one oxygen of the GLU47 (green or blue) binds at any given time. The oxygens exchange between GLU47, green to blue, can be observed in Fig. 6C at approximately 35 ns. In addition, the GLY45 oxygen distance to the Ca^{2+} fluctuates around a mean value of 5 Å. The third arrangement (6E and 6 F) shows that one of the oxygen atoms of GLU47 (green) is at ~2.3 Å from the Ca^{2+}. Large fluctuations are observed for the oxygens atoms in GLU42 (red-black), whereas the oxygen of GLY45 (orange) remains at a distance similar to the other oxygen of GLU47 (blue).

In relation with these amino acids, Bennet et al. reported the interaction between them and a calcium ion by X-ray crystallography (Bennett et al., 2016). In this work, an electrostatic barrier driven by Ca^{2+} for the GLY45 in coordination with GLU42 and GLU47 was proposed. However, as a final remark, the authors doubted about the strength of GLY45 role in this arrangement. In our simulations, the GLY45 residue is found at a longer distance from the calcium that the one reported by the X-ray studies. Moreover, here GLY45 appears to be repelled by the changes in the total force from the calcium ion and the GLU42 and GLU47 from adjacent connexins. This behavior supports Bennet et al. theory that GLY45 was not a stable participant on this complex network. These results exemplify the strength of un-constrained MD simulations to study the dynamic behavior of these kinds of systems that escapes some experimental approaches.

It is important to also notice that the interaction of GLU47 and calcium was studied by the means of quantum chemistry methods by Zonta et al. Zonta et al. (2014b). Through their calculations, the researchers explored GLU47, ARG75 and ARG184 with Ca^{2+} in a Cx26 hemichannel and their results proved that the post-translational glutamate GLU47 is a strong candidate to bind Ca^{2+} in the extracellular side on Cx26. However, the computational cost of the calculations is too high and then the procedure might be applicable exceptionally to confirm an argued mechanism of interaction, as the authors did.

Because Ca^{2+} ion regulation plays a key role in defining the physiological activity of the connexons we hypothesize that mutations in close proximity (in sequence or physical proximity, see also Methods section) of Ca^{2+} ion binding sites are more likely to cause pathological alterations. However, very little is known with respect to the molecular mechanisms of diseases associated with these variants. Fig. 7 shows the sequence of Cx26, where the Ca^{2+} binding sites and mutation sites obtained from ClinVar have been highlighted.

Fig. 7 shows that there are Ca^{2+} binding sites for which pathogenic variants have been reported, i.e. GLU120 and ASP159. Moreover, a number of calcium binding sites are one or two residues apart from a reported mutation site (García et al., 2016; Srinivas et al., 2017; Heathcote et al., 2000; Kelsell and Di W-L, 2001; Bavamian et al., 2009; Snoeckx et al., 2005). While these observations are important, it is also relevant to take into account the three-dimensional nature of our problem. Mutation sites that are far from calcium binding sites in the protein sequence may be in physical proximity and therefore, able to change calcium binding ability at the site. To study this issue, we labelled in the Cx26 structure the calcium binding sites and the mutations sites using a pairwise approach and visually identified potential regions of interest (see Fig. 8 for an example).

The summarization of these analysis is presented in Table 2, where we show all the possible regions of interaction between sites with reported pathogenic mutations (ClinVar) and Ca^{2+} binding sites found in the MD simulations. In all cases these results have been derived from visual inspection and using an inclusive criterion. Also, in Table 2 we associate our findings with the recently reported (García et al., 2016; Srinivas et al., 2017) functional state of Cx26 hemichannels, gap-junctions and pathological phenotypes (Snoeckx et al., 2005). It is important to notice that due to the three-dimensional approach used here

Table 2
Connexin sequences for which there are reported variants in ClinVar that are in proximity to binding sites identified in this study.

Sequences	Mutation reported in ClinVar	Ca+2 binding residues found in this work	GJC Function	HCs Function	Deafness Phenotype
GVNKH**S**(17)	G12R (+*) (Lee et al., 2009; García et al., 2015)	VAL226	(-)	(+)	S, Mild, Severe. KID/EKV
VLF(29)	V27I (Choi et al., 2011)	NONE	Normal	Normal	NS, HL and Normal
RIMILV(37)	V37I (García-Jaramillo et al., 2012)	ASP2	(-)	(-)	NS, Mild-Moderate, Severe
WGD(46)	W44C W44S D46E (Zhang et al., 2005; Martin et al., 1999; Zhang et al., 2011; Yum et al., 2010; Rouan et al., 2001; Choi et al., 2009; Bruzzone et al., 2001; Tekin et al., 2001)	GLU42	(-)	n.d.	NS, Severe to Profound, HL, Moderate, Severe
	G45E (Da et al., 2007; Sanchez and Verselis, 2014; Ha et al., 2010; Stong et al., 2006; Ogawa et al., 2014; Oguchi et al., 2005)		Normal	(+)	S, Profound. KID
NTLQPG(59)	G59 V (Palmada et al., 2006; Tóth et al., 2004)	ASP2 GLU42 GLU47 ASP50	n.d.	(-)	NS, Profound
YDH(66)	D66H (Zhang et al., 2011; Yum et al., 2010; Rouan et al., 2001)	NONE	n.d.	n.d.	Multilating keratoderma (No deafness reported)
ISHIRLWALQ(80)	R75Q R75W (Zhang et al., 2011; Yum et al., 2010; Marziano et al., 2003; Chen et al., 2005; Iossa et al., 2011)	ASP2 GLU42 GLU47 ASP50 ASP159	(-)	(-)	S, Severe to Profound. PPK
	W77R (Bruzzone et al., 2003; Bajaj et al., 2008; Carrasquillo et al., 1997)		(-)	n.d.	NS, Moderate to Profound
FVSTPALL(90)	V84 L (Bruzzone et al., 2003; Beltramello et al., 2005; Kenna et al., 2001; Wang et al., 2003; Ambrosi et al., 2010)	ASP2	Normal/No IP3 transfer	n.d.	NS. Profound
	T86R A88S L90P (Choi et al., 2009; Thönnissen et al., 2002; Cryns et al., 2004)		(-)	(-)	NS, Profound, Moderate to Profound, Mild to Moderate
	A88V (Iossa et al., 2011; Mhaske et al., 2013; Meigh et al., 2014)		n.d.	(+)	S, Severe to Profound. KID
MHV(95)	n.d.	NONE	n.d.	n.d.	NS.
EKK**R**(104)	n.d.	GLU114 ASP117 GLU119 GLU120	n.d.	n.d.	NS.
Punctual: E114 G R127H	E114 G R127H (Choi et al., 2011; Palmada et al., 2006; Tóth et al., 2004; Wang et al., 2003; Bicego et al., 2006; Posukh et al., 2005; Löffler et al., 2001)	GLU114 ASP117 GLU119 GLU121	(-)	(-)	NS, Severe to Profound, Profound
IEE(120)	DelE120 (Zhang et al., 2005; Bruzzone et al., 2003; Mani et al., 2009)	OVERLAP WITH GLU114 ASP117 GLU119 GLU120 VAL226	(-)	n.d.	NS, Severe to Profound
TQKVRIEG(130)	G130 A (Yong-Yi et al., 2007)	GLU114 ASP117 GLU119 GLU120 VAL226	n.d.	n.d.	NS.HL.
FRVIFEA(148)	R143Q (Zhang et al., 2011; Yum et al., 2010; Löffler et al., 2001; Meşe et al., 2004; Marlin et al., 2001)	NONE	(-)	n.d.	NS, Profound
	R143W (Palmada et al., 2006; Wang et al., 2003; Meşe et al., 2004; Man et al., 2007; Brobby and Muller-Myhsok, 1998)		(-)	(-)	NS, Profound
YVF(154)	V153I (Snoeckx et al., 2005)	ASP159	n.d.	n.d.	NS.HL. NS (No deafness reported)
YDG(160)	G160S (Zheng et al., 2018)	OVERLAP WITH ASP159	n.d.	n.d.	S.HL.KID
	D159 V (Gualandi et al., 2002)		n.d.	n.d.	NS.
RLVKC(169)	R165 W (Santos et al., 2005)	NONE	(-)	n.d.	NS, HL, Severe to Profound
VDC(180)	D179 N (Primignani et al., 2003)	NONE	(-)	n.d.	NS, HL, Severe to Profound
SRP(185)	R184 P R184Q (Snoeckx et al., 2005; Su et al., 2010)	NONE	(-)	n.d.	NS, HL, Severe to Profound
	S183 F (Ea et al., 2008)		(-)	n.d.	S, High Frequency HL. PPK
FTVFMIA(197)	M195 T A197S (Bai-Lin Wu et al., 2002; Hamelmann et al., 2001; Ambrosi et al., 2013; Meşe et al., 2008)	NONE	(-)	n.d.	NS, HL, Moderate, Profound
CIL(204)	C202 F (Kelsell and Di W-L, 2001)	NONE	n.d.	(-)	NS, Mild to Moderate
	I203 T (Han et al., 2008)		(-)	(-)	NS, HL, Profound
LL**I**(215)	L214 P (Hamelmann et al., 2001)	NONE	n.d.	n.d.	NS. HL

* Residues in bold have pathogenic mutations reported in ClinVar. The number between parentheses corresponds to the sequence number of the last amino acid listed.
& Ca^{+2} binding residues found in the MD simulations that have spatial proximity to the sequence with reported mutations.
S. Syndromic NS. Non-syndromic. HL. Hearing-loss. KID. Keratitis-ichthyosis-deafness. n.d. No-data available.
(+*) = Generate gain of HC function when they are expressed with wild type Cx26 or Cx43 (García et al., 2015).

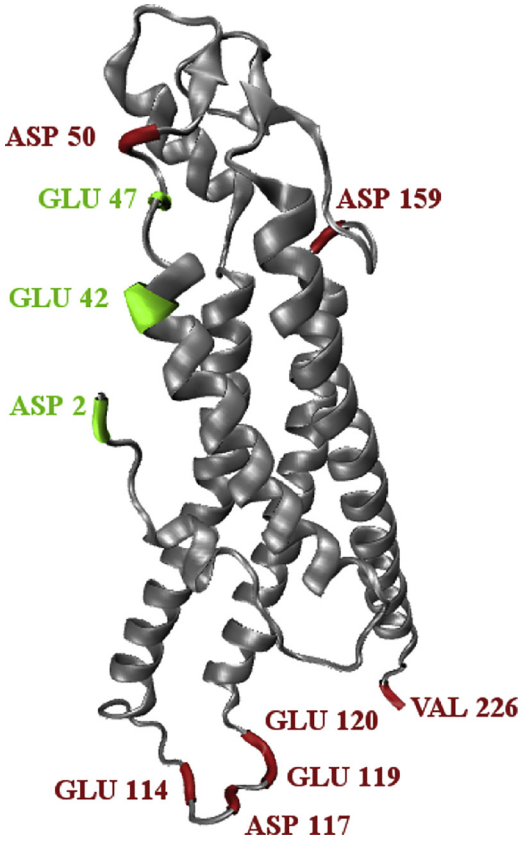

Fig. 9. Schematic representation of the connexin. The amino acids involved in calcium specific interaction sites were highlighted in red, the ones found with the first initial condition and those observed after adding eight Ca^{2+} inside the pore are in green (For interpretation of the references to colour in this figure legend, the reader is referred to the web version of this article).

to identify the possible associations between reported mutations and calcium-biding sites from the MD simulations, some mutations are at a distant region of the sequence from that where we find calcium binding sites. This is for example the case of G12R and VAL226 as exemplified in Fig. S19 of the supplementary material.

4. Conclusions

In this work, we carried out eight simulations considering different calcium concentration and initial conditions. Our results were able to capture interesting features of the calcium-connexon interaction. In particular we identified 10 amino acid involved in specific interaction sites, which are summarized them in Fig. 9. Besides the agreement that we found with the specific sites for calcium already defined in literature, in our work we identified novel ones and went forward capturing different kind of arrangements that could shed light to the interaction of calcium with Cx26. In addition, a summary of the number of calcium ions in relation with these residues is presented in Table S1 of the Supplementary Material.

Given the relevance of calcium in the physiopathology of conditions that affect the Cx26 connexon channel activity (García et al., 2016; Srinivas et al., 2017; Yeager and Harris, 2007) it is important to have an insight on the molecular interactions of these two key components. In this work, using calcium as a probe at high concentrations, we found the first indication of different calcium sites through the electron density profile. Further inspection at the molecular level helped us to find specific amino acid interactions with calcium and their dynamics. This interaction mainly occurs with the carboxyl groups of the amino acids, similar to what it was described for other compounds as it can be exemplified by the chelation mechanism of the calcium by the functional groups of the PAMAM and EDTA (Jones et al., 2016).

Molecular Dynamics simulations proved to be a powerful tool to explore a biological system at the molecular level. The identification of the specific sites where calcium could have an important role in the connexon structure is a step forward to understand the complex world of the intercellular communication. Moreover, by combining the MD results with known pathogenic mutation sites, we were able to find regions of the protein for which in depth studies of how mutations affect structure and dynamics of calcium binding may elucidate pathogenic pathways and perhaps identified potential therapeutic avenues.

We suggest further research, including MD simulation in mutated proteins, to further explore these systems, and dedicated in vitro experiments. While our work has been restricted to Cx26, the methods proposed here could be extended to other connexins for which experimental structures are available or by using 3D structure prediction approaches (Wen et al., 2017). Both, the connexinophaties understanding and the development of new therapies will benefit from the knowledge at the molecular level of these systems.

Conflict of interest

The authors report that they do not have any conflict of interest as related to the research reported in this paper.

Acknowledgements

The Center for High Performance Computing at The Utah University provided computer resources for High Performance Computing. JCF has been partially supported by the University of Utah Center for Clinical and Translational Science under NCATS Grant U01TR002538. NM and MBF have been partially supported by the University of Buenos Aires Grant 20020130100039BA and PIP CONICET 11220130100377. JMRA has been partialy supported by the Florencio Fiorini Foundation. MP have been partially supported by grants ANPCyT PICT2014- 3653, PIP CONICET0131-2014 and by the University of Buenos Aires Grant 20020130200138BA.

Appendix A. Supplementary data

Supplementary data associated with this article can be found, in the online version, at https://doi.org/10.1016/j.compbiolchem.2018.11.004.

References

Abraham, M.J., Murtola, T., Schulz, R., Páll, S., Smith, J.C., Hess, B., et al., 2015. Gromacs: high performance molecular simulations through multi-level parallelism from laptops to supercomputers. SoftwareX 1–2, 19–25. https://doi.org/10.1016/j.softx.2015.06.001. PubMed PMID: 22713035.

Albano, J.M.R., de Paula, E., Pickholz, M., 2018. In: Vakhrushev, A. (Ed.), Molecular Dynamics Simulations to Study Drug Delivery Systems. Molecular Dynamics IntechOpen.

Ambrosi, C., Boassa, D., Pranskevich, J., Smock, A., Oshima, A., Xu, J., et al., 2010. Analysis of four connexin26 mutant gap junctions and hemichannels reveals variations in hexamer stability. Biophys. J. 98, 1809–1819. https://doi.org/10.1016/j.bpj.2010.01.019. PubMed PMID: 20441744.

Ambrosi, C., Boassa, D., Pranskevich, J., Smock, A., Oshima, A., Xu, J., et al., 2013. Analysis of trafficking, stability and function of human connexin 26 gap junction channels … Supplemental Information. PLoS One 98, e70916.

Araya-Secchi, R., Perez-Acle, T., Kang, S.G., Huynh, T., Bernardin, A., Escalona, Y., et al., 2014. Characterization of a novel water pocket inside the human Cx26 hemichannel structure. Biophys. J. 107, 599–612. https://doi.org/10.1016/j.bpj.2014.05.037. PubMed PMID: 25099799.

Bai-Lin Wu, P., Lindeman, Neal, Va, Lip, 2002. Effectiveness of sequencing connexin 26 (GJB2) in cases of familial or sporadic childhood deafness referred for molecular diagnostic testing. Genet. Med. 4 (4), 279–288 10.109700125817-200207000-00006 PubMed PMID: 12172394.

Bajaj, Y., Sirimanna, T., Albert, D.M., Qadir, P., Jenkins, L., Bitner-Glindzicz, M., 2008. Spectrum of GJB2 mutations causing deafness in the British Bangladeshi population. Clin. Otolaryngol. 33, 313–318. https://doi.org/10.1111/j.1749-4486.2008.01754.x.

PubMed PMID: 18983339.
Batool, A., Yasmeen, S., Rashid, S., 2017. T8M mutation in connexin-26 impairs the connexon topology and shifts its interaction paradigm with lipid bilayer leading to non-syndromic hearing loss. J. Mol. Liq. 227 (C), 168–177. https://doi.org/10.1016/j.molliq.2016.12.018.
Bavamian, S., Klee, P., Allagnat, F., Haefliger, J.A., Meda, P., 2009. Connexins and secretion. Connexins: A Guide. Humana Press, Totowa, NJ, pp. 511–527.
Beltramello, M., Piazza, V., Bukauskas, F.F., Pozzan, T., Mammano, F., 2005. Impaired permeability to Ins(1,4,5)P3 in a mutant connexin underlies recessive hereditary deafness. Nat. Cell Biol. 7, 63–69. https://doi.org/10.1038/ncb1205. PubMed PMID: 15592461.
Bennett, M.V.L., Contreras, J.E., Bukauskas, F.F., Sáez, J.C., 2003. New roles for astrocytes: gap junction hemichannels have something to communicate. Trends Neurosci. 26, 610–617. https://doi.org/10.1016/j.tins.2003.09.008. PubMed PMID: 14585601.
Bennett, B.C., Purdy, M.D., Baker, K.A., Acharya, C., McIntire, W.E., Stevens, R.C., et al., 2016. An electrostatic mechanism for Ca(2+)-mediated regulation of gap junction channels. Nat. Commun. 7, 8770. https://doi.org/10.1038/ncomms9770. PubMed PMID: 26753910.
Best, R.B., Zhu, X., Shim, J., Lopes, P.E.M., Mittal, J., Feig, M., et al., 2012. Optimization of the additive CHARMM all-atom protein force field targeting improved sampling of the backbone and side-chain and Dihedral Angles. J. Chem. Theory Comput. 8, 3257–3273. https://doi.org/10.1021/ct300400x. PubMed PMID: 23341755.
Beyer, E.C., Berthoud, V.M., 2017. Gap junction structure: unraveled, but not fully revealed. F1000 Research 6, 568. https://doi.org/10.12688/f1000research.10490.1. PubMed PMID: 28529713.
Bicego, M., Beltramello, M., Melchionda, S., Carella, M., Piazza, V., Zelante, L., et al., 2006. Pathogenetic role of the deafness-related M34T mutation of Cx26. Hum. Mol. Genet. 15, 2569–2587. https://doi.org/10.1093/hmg/ddl184. PubMed PMID: 16849369.
Brobby, G.W., Muller-Myhsok, B., 1998. Connexin 26 R143W mutation associated with recessive nonsysndromic sensorineural deafness in Africa. N. Engl. J. Med. 338, 548–550. https://doi.org/10.1056/NEJM199802193380813.
Bruzzone, R., Gomès, D., Denoyelle, E., Duval, N., Perea, J., Veronesi, V., et al., 2001. Functional analysis of a dominant mutation of human connexin26 associated with nonsyndromic deafness. Cell Commun. Adhes. 8, 425–431 PubMed PMID: 12064630.
Bruzzone, R., Veronesi, V., Gomès, D., Bicego, M., Duval, N., Marlin, S., et al., 2003. Loss-of-function and residual channel activity of connexin26 mutations associated with non-syndromic deafness. FEBS Lett. 533, 79–88. https://doi.org/10.1016/S0014-5793(02)03755-9. PubMed PMID: 12505163.
Capener, C.E., Sansom, M.S.P., 2002. Molecular dynamics simulations of a K channel model: sensitivity to changes in ions, waters, and membrane environment. J. Phys. Chem. B 106, 4543–4551. https://doi.org/10.1021/jp0129986.
Carrasquillo, M.M., Zlotogora, J., Barges, S., Chakravarti, A., 1997. Two different connexin 26 mutations in an inbred kindred segregating non-syndromic recessive deafness: implications for genetic studies in isolated populations. Hum. Mol. Genet. 6, 2163–2172. https://doi.org/10.1093/hmg/6.12.2163. PubMed PMID: 9328482.
Chen, Y., Deng, Y., Bao, X., Reuss, L., Altenberg, G.A., 2005. Mechanism of the defect in gap-junctional communication by expression of a connexin 26 mutant associated with dominant deafness. Faseb J. 19, 1516–1518. https://doi.org/10.1096/fj.04-3491fje. PubMed PMID: 16009703.
Choi, S.-Y., Park, H.-J., Lee, K.Y., Dinh, E.H., Chang, Q., Ahmad, S., et al., 2009. Different functional consequences of two missense mutations in the GJB2 gene associated with non-syndromic hearing loss. Hum. Mutat. 30, E716–E727. https://doi.org/10.1002/humu.21036. PubMed PMID: 19384972.
Choi, S.-Y., Lee, K.Y., H-KH-J, Kim, H-KH-J, Kim, Chang, Q., Park, H.-J., et al., 2011. Functional evaluation of GJB2 variants in nonsyndromic hearing loss. Mol. Med. 17, 550–556. https://doi.org/10.2119/molmed.2010.00183. PubMed PMID: 21298213.
Cryns, K., Orzan, E., Murgia, A., Huygen, P.L.M., Moreno, F., del Castillo, I., et al., 2004. A genotype-phenotype correlation for GJB2 (connexin 26) deafness. J. Med. Genet. 41, 147–154. https://doi.org/10.1136/jmg.2003.013896. PubMed PMID: 14985372.
Da, Gerido, DeRosa, A.M., Richard, G., White, T.W., 2007. Aberrant hemichannel properties of Cx26 mutations causing skin disease and deafness. Am. J. Physiol. Cell Physiol. 293, C337–C345. https://doi.org/10.1152/ajpcell.00626.2006. PubMed PMID: 17428836.
Delmar, M., Makita, N., 2012. Cardiac connexins, mutations and arrhythmias. Curr. Opin. Cardiol. 27, 236–241. https://doi.org/10.1097/HCO.0b013e328352220e. PubMed PMID: 22382502.
Ea, de Zwart-Storm, van Geel, M., van Neer, Pa Fa, Steijlen, P.M., Martin, P.E., van Steensel, Ma M., 2008. A novel missense mutation in the second extracellular domain of GJB2, p.Ser183Phe, causes a syndrome of focal palmoplantar keratoderma with deafness. Am. J. Pathol. 173, 1113–1119. https://doi.org/10.2353/ajpath.2008.080049. PubMed PMID: 18787097.
Elias, L.A., Wang, D.D., Kriegstein, A.R., 2007. Gap junction adhesion is necessary for radial migration in the neocortex. Nature 448, 901–907. https://doi.org/10.1038/nature06063. PubMed PMID: 17713529.
Evans, W.H., Martin, P.E.M., 2002. Gap junctions: structure and function (Review). Mol. Membr. Biol. 19, 121–136. https://doi.org/10.1080/09687680210139839. PubMed PMID: 12126230.
Ewald, P.P., 1921. Die berechnung optischer und elektrostatisher gitterpotentiale. Ann. Phys. 64, 253–287.
Figueroa, X.F., Duling, B.R., 2009. Gap junctions in the control of vascular function. Antioxid. Redox Signal. 11, 251–266. https://doi.org/10.1089/ars.2008.2117. PubMed PMID: 18831678.
García, I.E., Maripillán, J., Jara, O., Ceriani, R., Palacios-Muñoz, A., Ramachandran, J., et al., 2015. Keratitis-ichthyosis-deafness syndrome-associated Cx26 mutants produce nonfunctional gap junctions but hyperactive hemichannels when Co-expressed with wild type Cx43. J. Invest. Dermatol. 135, 1338–1347. https://doi.org/10.1038/jid.2015.20. PubMed PMID: 25625422.
García, I.E., Prado, P., Pupo, A., Jara, O., Rojas-Gómez, D., Mujica, P., et al., 2016. Connexinopathies: a structural and functional glimpse. BMC Cell Biol. 17, S17. https://doi.org/10.1186/s12860-016-0092-x. PubMed PMID: 27228968.
García-Jaramillo, M., Calm, R., Bondia, J., Tarín, C., Vehí, J., 2012. Insulin dosage optimization based on prediction of postprandial glucose excursions under uncertain parameters and food intake. Comput. Methods Programs Biomed. 105, 61–69. https://doi.org/10.1016/j.cmpb.2010.08.007.
González, D., Gómez-Hernández, J.M., Barrio, L.C., 2006. Species specificity of mammalian connexin-26 to form open voltage-gated hemichannels. Faseb J. 20, 2329–2338. https://doi.org/10.1096/fj.06-5828com. PubMed PMID: 17077310.
Gualandi, F., Ravani, A., Berto, A., Sensi, A., Trabanelli, C., Falciano, F., et al., 2002. Exploring the clinical and epidemiological complexity of GJB2 -Linked deafness. Am. J. Med. Genet. 45, 38–45. https://doi.org/10.1002/ajmg.10621.
Ha, S.ánchez, Mese, G., Srinivas, M., White, T.W., Verselis, V.K., 2010. Differentially altered Ca2+ regulation and Ca2+ permeability in Cx26 hemichannels formed by the A40V and G45E mutations that cause keratitis ichthyosis deafness syndrome. J. Gen. Physiol. 136, 47–62. https://doi.org/10.1085/jgp.201010433. PubMed PMID: 20584891.
Hamelmann, C., Amedofu, G., Albrecht, K., Muntau, B., Gelhaus, A., 2001. Pattern of connexin 26 (GJB2) mutations causing sensorineural hearing impairment in Ghana. Hum. Mutat. 18 (84Á85) 18:84-5.
Han, S.H., Park, H.J., Kang, E.J., Ryu, J.S., Lee, A., Yang, Y.H., et al., 2008. Carrier frequency of GJB2 (connexin-26) mutations causing inherited deafness in the Korean population. J. Hum. Genet. 53, 1022–1028. https://doi.org/10.1007/s10038-008-0342-7. PubMed PMID: 19043807.
Hanner, F., Sorensen, C.M., Holstein-Rathlou, N.-H., Peti-Peterdi, J., 2010. Connexins and the kidney. Am. J. Physiol. Regul. Integr. Comp. Physiol. 298, R1143–55. https://doi.org/10.1152/ajpregu.00808.2009. PubMed PMID: 20164205.
Heathcote, K., Syrris, P., Carter, N.D., Patton, Ma., 2000. A connexin 26 mutation causes a syndrome of sensorineural hearing loss and palmoplantar hyperkeratosis (MIM 148350). J. Med. Genet. 37, 50–51. https://doi.org/10.1136/jmg.37.1.50. PubMed PMID: 10633135.
Herce, H.D., Garcia, A.E., Darden, T., 2007. The electrostatic surface term:(I) periodic systems. J. Chem. Phys. 126, 124106. https://doi.org/10.1063/1.2714527.
Hess, B., Kutzner, C., van der Spoel, D., Lindahl, E., 2008. GROMACS 4: algorithms for highly efficient, load balanced, and scalable molecular simulations. J. Chem. Theory Comput. 4, 435–447. https://doi.org/10.1021/ct700301q.
Hoover, W.G., 1985. Canonical dynamics: equilibrium phase-space distributions. Phys. Rev. 31, 1695–1697. https://doi.org/10.1103/PhysRevA.31.1695. PubMed PMID: 9895674.
Humphrey, W., Dalke, A., Schulten, K., 1996. VMD: visual molecular dynamics. J. Mol. Graph. 14, 33–38. https://doi.org/10.1016/0263-7855(96)00018-5. PubMed PMID: 8744570.
Hung, A., Yarovsky, I., 2011. Gap junction hemichannel interactions with zwitterionic lipid, anionic lipid, and cholesterol: molecular simulation studies. Biochemistry 50, 1492–1504. https://doi.org/10.1021/bi1004156. PubMed PMID: 21241055.
Iossa, S., Marciano, E., Franzé, A., 2011. GJB2 gene mutations in syndromic skin diseases with sensorineural hearing loss. Curr. Genomics 12, 475–785. https://doi.org/10.2174/138920211797904098. PubMed PMID: 22547955.
Jo, S., Kim, T., Iyer, V., Im, W., 2008. CHARMM GUI: a web based graphical user interface for CHARMM. J. Comput. Chem. 29, 1859–1865. https://doi.org/10.1002/jcc.20945.
Jones, D.E., Lund, A.M., Ghandehari, H., Facelli, J.C., 2016. Molecular dynamics simulations in drug delivery research: calcium chelation of G3.5 PAMAM dendrimers. Cogent Chem. 2, 1229830. https://doi.org/10.1080/23312009.2016.1229830.
Kabsch, W., 1976. A solution for the best rotation to relate two sets of vectors. Acta Crystallogr. Sect. A 32, 922–923. https://doi.org/10.1107/S0567739476001873. PubMed PMID: 96.
Kelsell, D.P., Di W-L, Houseman M.J., 2001. Connexin mutations in skin disease and hearing loss. Am. J. Hum. Genet. 68, 559–568. https://doi.org/10.1086/318803. PubMed PMID: 11179004.
Kelsell, D.P., Dunlop, J., Stevens, H.P., Lench, N.J., Liang, J.N., Parry, G., et al., 1997. Connexin 26 mutations in hereditary non-syndromic sensorineural deafness. Nature 387, 80–83. https://doi.org/10.1038/387080a0. PubMed PMID: 9139825.
Kenna, M.A., Wu, B.L., Cotanche, D.A., Korf, B.R., Rehm, H.L., 2001. Connexin 26 studies in patients with sensorineural hearing loss. Arch. Otolaryngol. Head Neck Surg. 127, 1037–1042 PubMed PMID: 11556849.
Kwon, T., Roux, B., Jo, S., Klauda, J.B., Harris, A.L., Bargiello, T.A., 2012. Molecular dynamics simulations of the Cx26 hemichannel: insights into voltage-dependent loop-gating. Biophys. J. 102, 1341–1351. https://doi.org/10.1016/j.bpj.2012.02.009. PubMed PMID: 22455917.
Kyle, J.W., Minogue, P.J., Thomas, B.C., DaL, Domowicz, Berthoud, V.M., Da, Hanck, et al., 2008. An intact connexin N-terminus is required for function but not gap junction formation. J. Cell. Sci. 121, 2744–2750. https://doi.org/10.1242/jcs.032482. PubMed PMID: 18664489.
Landrum, M.J., Lee, J.M., Riley, G.R., Jang, W., Rubinstein, W.S., Church, D.M., et al., 2014. ClinVar: public archive of relationships among sequence variation and human phenotype. Nucleic Acids Res. 42, D980–D985. https://doi.org/10.1093/nar/gkt1113. PubMed PMID: 24234437.
Lee, J.R., Derosa, A.M., White, T.W., 2009. Connexin mutations causing skin disease and deafness increase hemichannel activity and cell death when expressed in Xenopus oocytes. J. Invest. Dermatol. 129, 870–878. https://doi.org/10.1038/jid.2008.335. PubMed PMID: 18987669.

Locke, D., Koreen, I.V., Harris, A.L., 2006. Isoelectric points and post-translational modifications of connexin26 and connexin32. Faseb J. 20, 1221–1223. https://doi.org/10.1096/fj.05-5309fje. PubMed PMID: 16645047.

Löffler, J., Nekahm, D., Hirst-Stadlmann, A., Günther, B., Menzel, H.J., Utermann, G., et al., 2001. Sensorineural hearing loss and the incidence of Cx26 mutations in Austria. Eur. J. Hum. Genet. 9, 226–230. https://doi.org/10.1038/sj.ejhg.5200607. PubMed PMID: 11313763.

Lopez, W., Gonzalez, J., Liu, Y., Harris, A.L., Contreras, J.E., 2013. Insights on the mechanisms of Ca(2+) regulation of connexin26 hemichannels revealed by human pathogenic mutations (D50N/Y). J. Gen. Physiol. 142, 23–35. https://doi.org/10.1085/jgp.201210893. PubMed PMID: 23797420.

Lopez, W., Ramachandran, J., Alsamarah, A., Luo, Y., Harris, A.L., Contreras, J.E., 2016. Mechanism of gating by calcium in connexin hemichannels. Proc. Natl. Acad. Sci., 201609378. https://doi.org/10.1073/pnas.1609378113.

Mab, Vinken, Ta, Vanhaecke, Pa, Papeleu, Sa, Snykers, Ta, Henkens, Rogiers, Va., 2006. Connexins and their channels in cell growth and cell death. Cell. Signal. 18, 592–600. https://doi.org/10.1016/j.cellsig.2005.08.012.

Maeda, S., Tsukihara, T., 2011. Structure of the gap junction channel and its implications for its biological functions. Cell. Mol. Life Sci. 68, 1115–1129. https://doi.org/10.1007/s00018-010-0551-z.

Maeda, S., Nakagawa, S., Suga, M., Yamashita, E., Oshima, A., Fujiyoshi, Y., et al., 2009. Structure of the connexin 26 gap junction channel at 3.5 A resolution. Nature 458, 597–602. https://doi.org/10.1038/nature07869. PubMed PMID: 19340074.

Mahoney, M.W., Jorgensen, W.L., 2000. A five-site model for liquid water and the reproduction of the density anomaly by rigid, nonpolarizable potential functions. J. Chem. Phys. 112, 8910. https://doi.org/10.1063/1.481505. PubMed PMID: 86851200022.

Man, Y.K.S., Trolove, C., Tattersall, D., Thomas, A.C., Papakonstantinopoulou, A., Patel, D., et al., 2007. A deafness-associated mutant human connexin 26 improves the epithelial barrier in vitro. J. Membr. Biol. 218, 29–37. https://doi.org/10.1007/s00232-007-9025-0. PubMed PMID: 17581693.

Mani, R.S., Ganapathy, A., Jalvi, R., Srikumari Srisailapathy, C.R., Malhotra, V., Chadha, S., et al., 2009. Functional consequences of novel connexin 26 mutations associated with hereditary hearing loss. Eur. J. Hum. Genet. 17, 502–509. https://doi.org/10.1038/ejhg.2008.179. PubMed PMID: 18941476.

Marlin, S., Garabédian, E.N., Roger, G., Moatti, L., Matha, N., Lewin, P., et al., 2001. Connexin 26 gene mutations in congenitally deaf children: pitfalls for genetic counseling. Arch. Otolaryngol. Head Neck Surg. 127, 927–933 PubMed PMID: 11493200.

Martin, P.E.M., Coleman, S.L., Casalotti, S.O., Forge, A., Howard Evans, W., 1999. Properties of Connexin26 gap junctional proteins derived from mutations associated with non-syndromal heriditary deafness. Hum. Mol. Genet. 8, 2369–2376. https://doi.org/10.1093/hmg/8.13.2369. PubMed PMID: 10556284.

Marziano, N.K., Casalotti, S.O., Portelli, A.E., Becker, D.L., Forge, A., 2003. Mutations in the gene for connexin 26 (GJB2) that cause hearing loss have a dominant negative effect on connexin 30. Hum. Mol. Genet. 12, 805–812. https://doi.org/10.1093/hmg/ddg076. PubMed PMID: 12668604.

Meigh, L., Hussain, N., Mulkey, D.K., Dale, N., 2014. Connexin26 hemichannels with a mutation that causes KID syndrome in humans lack sensitivity to CO2. eLife 3, e04249. https://doi.org/10.7554/eLife.04249. PubMed PMID: 25422938.

Meşe, G., Londin, E., Mui, R., Brink, P.R., White, T.W., 2004. Altered gating properties of functional Cx26 mutants associated with recessive non-syndromic hearing loss. Hum. Genet. 115, 191–199. https://doi.org/10.1007/s00439-004-1142-6. PubMed PMID: 15241677.

Meşe, G., Valiunas, V., Brink, P.R., White, T.W., 2008. Connexin26 deafness associated mutations show altered permeability to large cationic molecules. Am. J. Physiol. Cell Physiol. 295, C966–74. https://doi.org/10.1152/ajpcell.00008.2008. PubMed PMID: 18684989.

Mhaske, P.V., Na, Levit, Li, L., Wang, H.-Z., Lee, J.R., Shuja, Z., et al., 2013. The human Cx26-D50A and Cx26-A88V mutations causing keratitis-ichthyosis-deafness syndrome display increased hemichannel activity. Am. J. Physiol. Cell Physiol. 304, C1150–8. https://doi.org/10.1152/ajpcell.00374.2012. PubMed PMID: 23447037.

Nemoto-Hasebe, I., Akiyama, M., Yamada, N., Inoue, Y., Touge, C., Shimizu, H., 2008. Keratitis-ichthyosis-deafness syndrome lacking subjective hearing impairment. Acta Derm. Venereol. 88, 406–408. https://doi.org/10.2340/00015555-0457. PubMed PMID: 18709320.

Nielsen, M.S., Axelsen, L.N., Sorgen, P.L., Verma, V., Delmar, M., Holstein-Rathlou, N.-H., 2012. Gap junctions. Compr. Physiol. 2, 1981–2035. https://doi.org/10.1002/cphy.c110051. PubMed PMID: 23723031.

Nosé, S., 1984. A unified formulation of the constant temperature molecular dynamics methods. J. Chem. Phys. 81, 511. https://doi.org/10.1063/1.447334.

Ogawa, Y., Takeichi, T., Kono, M., Hamajima, N., Yamamoto, T., Sugiura, K., et al., 2014. Revertant mutation releases confined lethal mutation, opening Pandora's Box: a novel genetic pathogenesis. PLoS Genet. 10, e1004276. https://doi.org/10.1371/journal.pgen.1004276. PubMed PMID: 24785414.

Oguchi, T., Ohtsuka, A., Hashimoto, S., Oshima, A., Abe, S., Kobayashi, Y., et al., 2005. Clinical features of patients with GJB2 (connexin 26) mutations: severity of hearing loss is correlated with genotypes and protein expression patterns. J. Hum. Genet. 50, 76–83. https://doi.org/10.1007/s10038-004-0223-7. PubMed PMID: 15700112.

Oshima, A., 2014. Structure and closure of connexin gap junction channels. FEBS Lett. 588, 1230–1237. https://doi.org/10.1016/j.febslet.2014.01.042. PubMed PMID: 24492007.

Palmada, M., Schmalisch, K., Böhmer, C., Schug, N., Pfister, M., Lang, F., et al., 2006. Loss of function mutations of the GJB2 gene detected in patients with DFNB1-associated hearing impairment. Neurobiol. Dis. 22, 112–118. https://doi.org/10.1016/j.nbd.2005.10.005. PubMed PMID: 16300957.

Pantano, S., Zonta, F., Mammano, F., 2008. A fully atomistic model of the Cx32 connexon. PLoS One 3, 1–11. https://doi.org/10.1371/journal.pone.0002614. PubMed PMID: 18648547.

Parrinello, M., Rahman, A., 1982. Strain fluctuations and elastic constants. J. Chem. Phys. 76, 2662–2666. https://doi.org/10.1063/1.443248. PubMed PMID: 25246403.

Pasenkiewicz-Gierula, M., Takaoka, Y., Miyagawa, H., Kitamura, K., Kusumi, A., 1999. Charge pairing of headgroups in phosphatidylcholine membranes: a molecular dynamics simulation study. Biophys. J. 76, 1228–1240. https://doi.org/10.1016/S0006-3495(99)77286-3. PubMed PMID: 10049307.

Peracchia, C., 2004. Chemical gating of gap junction channels: roles of calcium, pH and calmodulin. Biochim. Biophys. Acta Biomembr. 1662, 61–80. https://doi.org/10.1016/j.bbamem.2003.10.020. PubMed PMID: 15033579.

Pettersen, E.F., Goddard, T.D., Huang, C.C., Couch, G.S., Greenblatt, D.M., Meng, E.C., et al., 2004. UCSF Chimera–a visualization system for exploratory research and analysis. J. Comput. Chem. 25 (13), 1605–1612. https://doi.org/10.1002/jcc.20084. Epub 2004/07/21 PubMed PMID: 15264254.

Pickholz, M., Fernandes Fraceto, L., de Paula, E., 2008. Distribution of neutral prilocaine in a phospholipid bilayer: insights from molecular dynamics simulations. Int. J. Quantum Chem. 108, 2386–2391. https://doi.org/10.1002/qua.21767.

Posukh, O., Pallares-Ruiz, N., Tadinova, V., Osipova, L., Claustres, M., Roux, A.-F., 2005. First molecular screening of deafness in the Altai Republic population. BMC Med. Genet. 6, 12. https://doi.org/10.1186/1471-2350-6-12. PubMed PMID: 15790391.

Pravda, L., Sehnal, D., Tousek, D., Navratilova, V., Bazgier, V., Berka, K., et al., 2018. MOLEonline: a web-based tool for analyzing channels, tunnels and pores (2018 update). Nucleic Acids Res. 46 (W1), W368–w373. https://doi.org/10.1093/nar/gky309. Epub 2018/05/03, PubMed PMID: 29718451; PubMed Central PMCID: PMCPMC6030847.

Primignani, P., Castorina, P., Sironi, F., Curcio, C., Ambrosetti, U., Coviello, D.A., 2003. A novel dominant missense mutation–D179N–in the GJB2 gene (Connexin 26) associated with non-syndromic hearing loss. Clin. Genet. 63, 516–521 079 [pii]. PubMed PMID: 12786758.

Rouan, F., White, T.W., Brown, N., aM, Taylor, Lucke, T.W., Paul, D.L., et al., 2001. Trans-dominant inhibition of Connexin-43 by mutant Connexin-26: implications for dominant connexin disorders affecting epidermal differentiation. J. Cell. Sci. 114, 2105–2113 PubMed PMID: 11493646.

Sanchez, H.A., Verselis, V.K., 2014. Aberrant Cx26 hemichannels and keratitis-ichthyosis-deafness syndrome: insights into syndromic hearing loss. Front. Cell. Neurosci. 8, 354. https://doi.org/10.3389/fncel.2014.00354. PubMed PMID: 25386120.

Santos, R.L.P., Wajid, M., Pham, T.L., Hussan, J., Ali, G., Ahmad, W., et al., 2005. Low prevalence of Connexin 26 (GJB2) variants in Pakistani families with autosomal recessive non-syndromic hearing impairment. Clin. Genet. 67, 61–68. https://doi.org/10.1111/j.1399-0004.2005.00379.x. PubMed PMID: 15617550.

Scott, C.A., Tattersall, D., O'Toole, E.A., Kelsell, D.P., 2012. Connexins in epidermal homeostasis and skin disease. Biochim. Biophys. Acta Biomembr. 1818, 1952–1961. https://doi.org/10.1016/j.bbamem.2011.09.004. PubMed PMID: 21933662.

Snoeckx, R.L., Huygen, P.L., Feldmann, D., Marlin, S., Denoyelle, F., Waligora, J., et al., 2005. GJB2 mutations and degree of hearing loss: a multicenter study. Am. J. Hum. Genet. 77, 945–957. https://doi.org/10.1086/497996. PubMed PMID: 16380907.

Srinivas, M., Verselis, V.K., White, T.W., 2017. Human diseases associated with connexin mutations. Biochim. Biophys. Acta (BBA) – Biomembr. https://doi.org/10.1016/j.bbamem.2017.04.024. PubMed PMID: 28457858.

Stong, B.C., Chang, Q., Ahmad, S., Lin, X., 2006. A novel mechanism for connexin 26 mutation linked deafness: cell death caused by leaky gap junction hemichannels. Laryngoscope 116, 2205–2210. https://doi.org/10.1097/01.mlg.0000241944.77192.d2. PubMed PMID: 17146396.

Su, C.-C., Li, S.-Y., Su, M.-C., Chen, W.-C., Yang, J.-J., 2010. Mutation R184Q of connexin 26 in hearing loss patients has a dominant-negative effect on connexin 26 and connexin 30. Eur. J. Hum. Genet. 18, 1061–1064. https://doi.org/10.1038/ejhg.2010.50. PubMed PMID: 20442751.

Tekin, M., Arnos, K.S., Xia, X.J., Oelrich, M.K., Liu, X.Z., Nance, W.E., et al., 2001. W44C mutation in the connexin 26 gene associated with dominant non-syndromic deafness. Clin. Genet. 59, 269–273. https://doi.org/10.1034/j.1399-0004.2001.590409.x. PubMed PMID: 11298683.

Thönnissen, E., Rabionet, R., Arbonès, M.L., Estivill, X., Willecke, K., Ott, T., 2002. Human connexin26 (GJB2) deafness mutations affect the function of gap junction channels at different levels of protein expresion. Hum. Genet. 111, 190–197. https://doi.org/10.1007/s00439-002-0750-2. PubMed PMID: 12189493.

Tóth, T., Kupka, S., Haack, B., Riemann, K., Braun, S., Fazakas, F., et al., 2004. GJB2 mutations in patients with non-syndromic hearing loss from Northeastern Hungary. Hum. Mutat. 23, 631–632. https://doi.org/10.1002/humu.9250. PubMed PMID: 15146474.

Trosko, J.E., Ruch, R.J., 1998. Cell-cell communication in carcinogenesis. Front Biosci. 3, d208–36. https://doi.org/10.2741/A275. PubMed PMID: 9458335.

Vendome, J., Posy, S., Jin, X., Bahna, F., Ahlsen, G., Shapiro, L., et al., 2011. Molecular design principles underlying β-strand swapping in the adhesive dimerization of cadherins. Nat. Struct. Mol. Biol. 18, 693–700. https://doi.org/10.1016/j.biotechadv.2011.08.021.Secreted. PubMed PMID: 1000000221.

Villanelo, F., Escalona, Y., Pareja-Barrueto, C., Garate, J.A., Skerrett, I.M., Perez-Acle, T., 2017. Accessing gap-junction channel structure-function relationships through molecular modeling and simulations. BMC Cell Biol. 18, 5. https://doi.org/10.1186/s12860-016-0121-9.

Vinken, M., 2015. Introduction: connexins, pannexins and their channels as gatekeepers of organ physiology. Cell. Mol. Life Sci. 72, 2775–2778. https://doi.org/10.1007/s00018-015-1958-3.

Wang, H.L., Chang, W.T., Li, A.H., Yeh, T.H., Wu, C.Y., Chen, M.S., et al., 2003. Functional analysis of connexin-26 mutants associated with hereditary recessive

deafness. J. Neurochem. 84, 735–742. https://doi.org/10.1046/j.1471-4159.2003.01555.x. PubMed PMID: 12562518.
Wen, J., Scoles, D.R., Facelli, J.C., 2017. Effects of the enlargement of polyglutamine segments on the structure and folding of ataxin-2 and ataxin-3 proteins. J. Biomol. Struct. Dyn. 35, 504–519. https://doi.org/10.1080/07391102.2016.1152199. PubMed PMID: 26861241.
Wu, Y., Tepper, H.L., Voth, G.A., 2006. Flexible simple point-charge water model with improved liquid-state properties. J. Chem. Phys. 124, 024503. https://doi.org/10.1063/1.2136877. PubMed PMID: 16422607.
Wu, E.L., Cheng, X., Jo, S., Rui, H., Song, K.C., Dávila-Contreras, E.M., et al., 2014. CHARMM-GUI Membrane Builder toward realistic biological membrane simulations. J. Comput. Chem. 35, 1997–2004. https://doi.org/10.1002/jcc.23702.
Yeager, M., Harris, A.L., 2007. Gap junction channel structure in the early 21st century: facts and fantasies. Curr. Opin. Cell Biol. 19, 521–528. https://doi.org/10.1016/j.ceb.2007.09.001. PubMed PMID: 17945477.
Yong-Yi, Y., Pu, D., Fei, Y., Xiu-Hui, Z., Hui-Jun, Y., Dong-Yi, H., et al., 2007. GJB2 mutation spectrum in Inner Mongolia and its comparison with other Asian populations. J. Otol. 2, 81–91.
Yum, S.W., Zhang, J., Scherer, S.S., 2010. Dominant connexin26 mutants associated with human hearing loss have trans-dominant effects on connexin30. Neurobiol. Dis. 38, 226–236. https://doi.org/10.1016/j.nbd.2010.01.010. PubMed PMID: 20096356.
Zhang, Y., Tang, W., Ahmad, S., Ja, Sipp, Chen, P., Lin, X., 2005. Gap junction-mediated intercellular biochemical coupling in cochlear supporting cells is required for normal cochlear functions. Proc. Natl. Acad. Sci. U. S. A. 102, 15201–15206. https://doi.org/10.1073/pnas.0501859102. PubMed PMID: 16217030.
Zhang, J., Scherer, S.S., Yum, S.W., 2011. Dominant Cx26 mutants associated with hearing loss have dominant-negative effects on wild type Cx26. Mol. Cell. Neurosci. 47, 71–78. https://doi.org/10.1016/j.mcn.2010.10.002. PubMed PMID: 21040787.
Zheng, J., Ying, Z., Cai, Z., Sun, D., He, Z., Gao, Y., et al., 2015. GJB2 mutation spectrum and genotype-phenotype correlation in 1067 Han Chinese subjects with non-syndromic hearing loss. PLoS One(10), e0128691. https://doi.org/10.1371/journal.pone.0128691. PubMed PMID: 26043044.
Zonta, F., Polles, G., Zanotti, G., Mammano, F., 2012a. Permeation pathway of homomeric connexin 26 and connexin 30 channels investigated by molecular dynamics. J. Biomol. Struct. Dyn. 29, 985–998. https://doi.org/10.1080/073911012010525027. PubMed PMID: 22292956.
Zonta, F., Polles, G., Zanotti, G., Mammano, F., 2012b. Permeation pathway of homomeric connexin 26 and connexin 30 channels investigated by molecular dynamics. J. Biomol. Struct. Dyn. 29 (5), 985–998. https://doi.org/10.1080/073911012010525027.
Zonta, F., Buratto, D., Cassini, C., Bortolozzi, M., Mammano, F., 2014a. Molecular dynamics simulations highlight structural and functional alterations in deafness-related M34T mutation of connexin 26. Front. Physiol. 5 (March), 1–9. https://doi.org/10.3389/fphys.2014.00085. PubMed PMID: 24624091.
Zonta, F., Mammano, F., Torsello, M., Fortunati, N., Orian, L., Polimeno, A., 2014b. Role of gamma carboxylated Glu47 in connexin 26 hemichannel regulation by extracellular Ca^{2+}: insight from a local quantum chemistry study. Biochem. Biophys. Res. Commun. 445, 10–15. https://doi.org/10.1016/j.bbrc.2014.01.063. PubMed PMID: 24468086.